Photoacoustic Fourier transform infrared spectroscopy of nanoporous SiO_x/Si thin films with varying porosities

D.-Q. Yang, M. Meunier, and E. Sacher[a)]
Regroupement Québécois de Matériaux de Pointe and Département de Génie Physique, École Polytechnique de Montréal, Casier Postal 6079, Succursale Centre-Ville, Montréal, Québec H3C 3A7, Canada

(Received 22 February 2005; accepted 21 October 2005; published online 9 December 2005)

Nanostructured SiO_x/Si thin films, over a large range of porosities, were deposited by the excimer laser ablation (KrF, 248 nm) of Si targets in He; they have been characterized by photoacoustic Fourier transform infrared spectroscopy, which necessitates exposure to air with subsequent oxidation. In particular, the IR Si–O–Si asymmetric stretching region, from 1000 to 1300 cm^{-1}, has been found to be composed of four components: P_1 at 1045 cm^{-1}, P_2 at 1060 cm^{-1}, P_3 at 1090 cm^{-1}, and P_4 at 1170 cm^{-1}. The photoacoustic signals were enhanced with increasing film porosity, as previously found for larger scale porous materials; those for P_{2-4} also correlated with similar increases in the O–H and $C–H_n$ surface contaminant stretching peaks, indicating their sources to be in the surface region. We demonstrate that the experimental data fully support a previously proposed theoretical relationship, originally developed for powders. © *2005 American Institute of Physics*. [DOI: 10.1063/1.2138376]

I. INTRODUCTION

Nanoporous Si thin films have attracted much interest over the last decade because they exhibit visible photoluminescence (PL) with quantum efficiencies of up to a few percent at room temperature, making them attractive materials for optoelectronic and biomedical device applications.[1,2] Nanostructured Si prepared under different conditions exhibit PL of varying intensities, wavelengths, and band shapes.[3–9] Although the quantum confinement model of PL[10,11] can accommodate some of the experimental data, they can equally well be explained by surface chemical composition [e.g., siloxane derivatives[12] and SiH_2 (Ref. 13)], defects (e.g., in the surface oxide[14] or at the SiO_x/Si interface[15,16]), surface-bonded chemical moieties,[4,9,12–18] and surface electronic states.[18]

There are many analytical tools available to characterize surfaces and interfaces of these materials. For example, x-ray photoelectron (XPS) and Fourier transform infrared (FTIR) spectroscopies have been widely used to characterize Si nanostructured materials.[2,6,9,19–25] However, knowledge gathered from these techniques has only provided limited information on the understanding of the origin of PL.

While many techniques have been used to produce porous Si,[19–21] pulsed laser ablation has the advantage over other methods in producing contaminant-free thin films[22,26–32]. The laser ablation of a silicon target, in residual He, leads to the deposition of nanoporous thin films. Because most of the kinetic energy of the ablated Si atoms and clusters is absorbed by the He gas, the tendency for larger particle growth is minimized. The microstructures formed depend on the parameters such as the gas pressure, sample-target distance, substrate temperature, laser power, wavelength, etc., but all lead to a typical nanoparticle size of ~5 nm.[31,33–35] These porous Si films are rapidly oxidized to SiO_x/Si on exposure to air at room temperature,[33–35] this oxidation being one of the most important factors for the production of the PL.

As we have noted,[32] the PL previously exhibited by Si thin films that were laser ablated in noble gases has produced conflicting results: some workers found that the PL was nearly independent of the preparation conditions,[27–29] while others found a strong experimental dependence.[31,32,36] Such films, produced by different groups, using different conditions, may well differ in chemical structure.

Infrared (IR) spectroscopy is often used in the determination of chemical structure, in that the local chemical groups are characterized by their vibrational frequencies. In the case of SiO_x, the band of frequencies between 1000 and 1300 cm^{-1} is clearly identified with the presence of Si–O–Si vibrations.[37] Several peaks are generally present in this region, whose attributions are necessary to an understanding of the chemical structure of the particular SiO_x sample under study. Unfortunately, the literature is not in agreement with these attributions. This is made clear by perusing a representative sampling of two decades of experimental results of SiO_x,[38–67]using data obtained on oxidized Si, siloxanes, and silsesquioxanes, both porous and nonporous, and produced by methods such as surface oxidation, plasma deposition, electrochemical etching, etc. These findings, which we do not tabulate here, are characterized by disagreements as to the number of peaks (2–5), whether their sources are local (Si–O–Si) or longer-range (LO and TO) vibrational modes, and their attributions (cyclic, long chain, hydroxyl terminated, etc.).

Much of this inconsistency is certainly due to the different methods of sample preparation used, and the resulting differences in the chemical structures obtained. Thus, it would appear that attempting to attribute these peaks by reference to the literature has little to offer. Rather, one must

[a)]Electronic mail: edward.sacher@polymtl.ca

submit one's own samples to controlled conditions that are well understood, and make attributions based on their effects on the peaks under study.

Conventional Fourier transform infrared (FTIR) spectroscopy has been used to explore porous SiO_x/Si thin-film microstructures in an effort to understand the origin of PL.[43,44,47,52,54,63] On the other hand, photoacoustic (PA) FTIR has received little such attention,[45,68,69] including an early study on micrometer-sized silica power during the development of theoretical PA-FTIR models.[68,69] More recently PA-FTIR was used to measure the thermal conductivity of porous Si layers produced by wet chemistry.[70]

Here, we present PA-FTIR spectral data on nanoporous Si. This system has the advantage of surface and near surface sensitivities, over a range of He deposition pressures previously found to strongly affect the porosities of the Si films deposited, and to exhibit broad PL patterns with varying peak intensities and positions.[18,31].

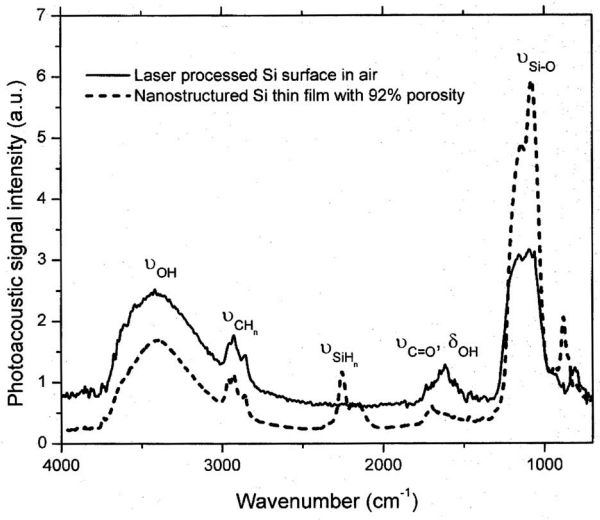

FIG. 1. Representative PA-FTIR spectra of nanoporous SiO_x/Si thin films, over the range of 700–4000 cm^{-1}.

II. EXPERIMENT

Nanoporous Si thin-film deposition was carried in a high-vacuum laser ablation deposition system, using the KrF laser ablation (GSI Lumonics, Inc., PulseMaster™ PM-800, $\lambda = 248$ nm at 20 Hz, with a 20 ns full width at half maximum) of a Si target in a high-purity He ambient. The laser radiation was focused on a spot 2×1 mm^2 on the target at an incident angle of 45°, giving a radiation intensity of $\sim 4 \times 10^8$ W/cm^2, while the target, at a distance of ~3 cm from the substrate, was rotated at 3 rps. The base pressure in the preparation chamber was below 5×10^{-7} torr and the He pressure was varied between 0.1 and 8 torr by adjusting the He mass flow meter. All were deposited at the same time using the same laser conditions, so that their deposited masses were similar. The film mass thickness (thickness at zero porosity) was kept constant at 200 nm, although the actual thicknesses differed up to 2 μm because of the porosity differences, which were controlled by the He pressure during deposition.

The porosities were determined by specular x-ray reflectivity (SXRR), whose details may be found in a previous publication from our laboratory.[31] On exposure to air, these films rapidly oxidize to SiO_x/Si, even during the short transfer time required for analysis, with the oxidation behavior[71,72] depending on both exposure time and film porosity. The samples used for the PA-FTIR study were exposed to air for at least 2 months because such exposure gave materials stable to further oxidation.[72]

PA-FTIR spectra were obtained using a He-purged MTEC 300 photoacoustic cell in a Bio-Rad FTS 6000 spectrometer. The 5 kHz modulation frequency used probed the entire sample thickness. The spectral resolution was set at 4 cm^{-1}.

III. RESULTS

A typical PA-FTIR spectrum, over the range of 700–4000 cm^{-1}, is shown in Fig. 1. One sees the results of atmospheric reaction: water adsorption is demonstrated by the sharp O–H stretching peak at ~3750 cm^{-1} (free –OH) and the broad O–H stretching peak at ~3400 cm^{-1} (hydrogen-bonded –OH). Further, the adsorption of airborne hydrocarbons is indicated by the $C-H_n$ stretching peaks near 2900 cm^{-1}.

The peaks near 2100 cm^{-1}, found for nanoporous thin films with high porosities, indicate the presence of SiH_n ($Si-H_n$ stretching) and, possibly, hydrocarbon (C═C stretching). Peaks near 1700 cm^{-1} indicate the presence of adsorbed water (H_2O deformation) and oxidized hydrocarbons (C═O stretching). Oxide formation is signaled by the broadband of Si–O–Si stretching peaks in the range of 1000–1300 cm^{-1}. In addition, the Si, laser processed in air, has a Si–O–Si bending peak at ~800 cm^{-1}, while the nanoporous Si, laser processed in He, has a peak near 880 cm^{-1}, previously attributed to Si rings isolated by oxygen;[73] we have found this peak only for highly porous films.

The Si–O–Si stretching peaks, in the range of 1000–1300 cm^{-1}, have received much study, partly because their high IR intensities made them so easy to study. Typical spectra, at several porosities, are found in Fig. 2(a); for purposes of comparison, Si wafers treated in various ways[74,75] are found (samples A–F) in Fig. 2(b), whose sources are described in the figure caption. It is clear that (1) all can be fit with the same four component peaks at 1045 cm^{-1} (P_1), 1060 cm^{-1} (P_2), 1090 cm^{-1} (P_3), and 1170 cm^{-1} (P_4); a typical deconvolution is found in Fig. 2(c), with standard Gaussian functions having the same full width at half maximum (FWHM) value (30 ± 2 cm^{-1}), except for P_4 (60 ± 2 cm^{-1}), and (2) their relative peak areas are dependent on porosity (Fig. 3) and surface treatment.

The PA-FTIR signal intensity of each of these peaks is noticeably enhanced with increasing porosity. An example is found in Fig. 3 for the P_4 peak (1170 cm^{-1}) area. The other absorption bands exhibit similar behavior; these amplitude relationships are all semilogarithmic: $\log P_1 \propto 0.020 \times$ porosity and $\log P_{2-4} \propto 0.029 \times$ porosity (while proportionalities are given rather than equalities, it is clear that the slope of $\log P_1$ differs from those of $\log P_{2-4}$). The *ratios* of

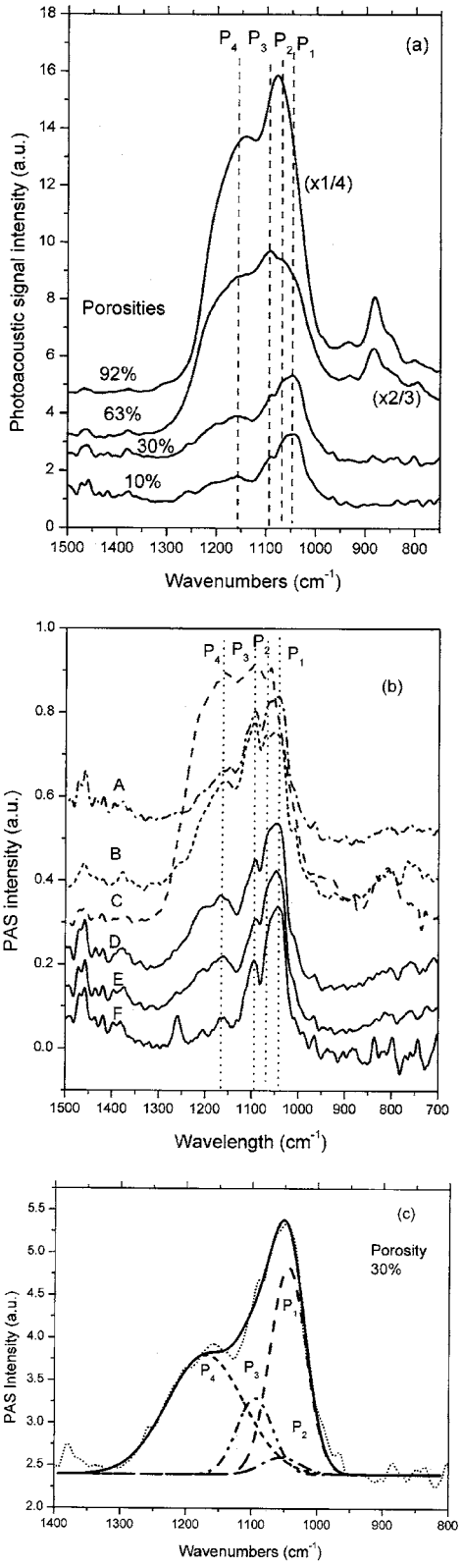

FIG. 2. PA-FTIR spectra of the Si–O–Si stretching region of (a) nanoporous SiO_x/Si thin films and (b) variously treated Si thin films, prepared for other studies, and used for purposes of comparison [including A, 5 nm Au, dc sputtered onto a native oxide-covered Si wafer surface; B, 3 nm Au, evaporated onto an O_2 plasma-treated Si wafer surface; C, SiO_x microtrees formed on Si by KrF excimer laser radiation (248 nm) in air Ref. 75; D, 3 nm Au, evaporated onto a native oxide-covered Si wafer surface; E, an untreated native oxide-covered Si wafer; F, a high-temperature thermally growth 250 nm SiO_2 thin film on Si]; (c) a typical deconvolution of $\nu_{Si-O-Si}$.

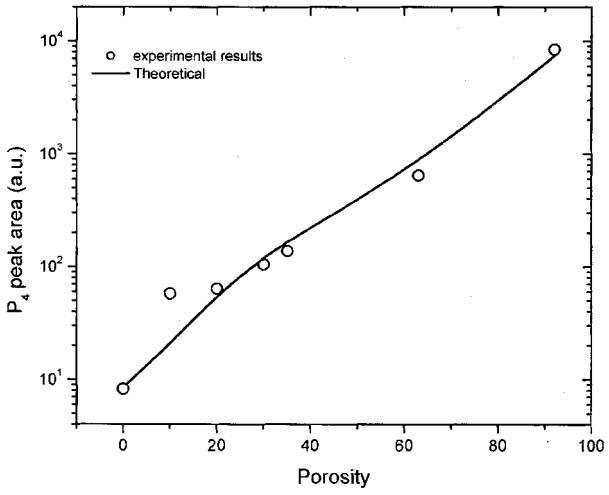

FIG. 3. Photoacoustic peak area of the P_4 Si–O–Si component peak of nanoporous SiO_x/Si thin films as a function of porosity. The line predicted by the theoretical model, using Eq. (1) (Ref. 69), and taking the SiO_x thickness into account[72], is also shown.

P_{2-4} to P_1 all increase with porosity (Fig. 4), as expected from the differing slopes, indicating that P_{2-4} are more porosity sensitive than P_1. In addition, the intensities of both the O–H stretching peak at $\sim 3400\ cm^{-1}$, and the $C-H_n$ stretching peaks at $\sim 2900\ cm^{-1}$ increase with porosity (not shown) with slopes identical to those of P_{2-4}.

IV. DISCUSSION

A. Surface-volume distribution of Si–O–Si peaks

Our experimental data, in Fig. 2, clearly indicate that there are four discernable components contributing to the local Si–O–Si stretching vibrations. The components maintain their positions for all the samples in Fig. 2, with P_1 appearing to depend less on the SiO_x porosity than P_{2-4}. The fact that both the O–H and $C-H_n$ stretching peaks are due to surface depositions, and have porosity-dependent slopes essentially identical to those of P_{2-4} indicates that P_{2-4} have their origins at the free surface. This is consistent with pre-

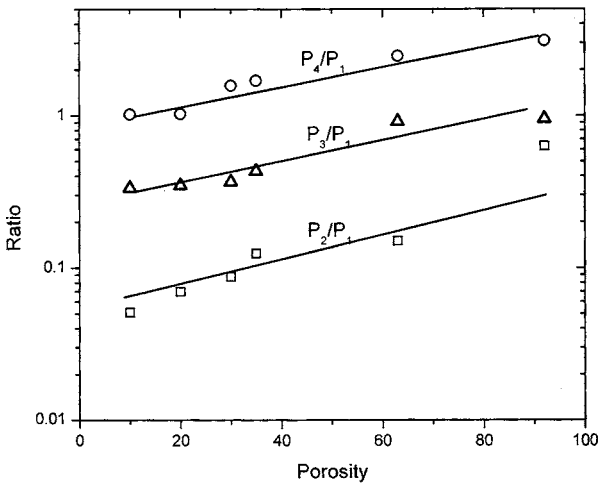

FIG. 4. The $P_2:P_1$, $P_3:P_1$, and $P_4:P_1$ component peak intensity ratios of nanoporous SiO_x/Si thin films as a function of porosity.

vious FTIR observations[45] of silicon dioxide thin films with different porosities, deposited by a liquid-phase-deposition technique. The presence of *three* adjacent surface-related peaks suggests slight differences in their structures, possibly due to –OH and $-CH_n$ terminations and/or short-range-disordered Si–O–Si chain/cyclic surface structures.[37] As mentioned earlier, they have already been characterized in the literature[38–67] by disagreements as to (a) the number of peaks (2–5), (b) their sources, which have been variously suggested to be local (Si–O–Si) or longer-range (LO and TO) vibrational modes, and (c) their attributions (cyclic, long chain, hydroxyl terminated, etc.). While the present results are able to indicate their surface and volume contributions, they bring us no closer to attributing them with any precision.

It is interesting to note that the band at 880 cm^{-1} (with a shoulder at lower wave numbers), which has been attributed to silicon ring configurations isolated by oxygen atoms,[73] as well as the Si–O–Si bending peak at 800 cm^{-1}, is not seen at low porosities. The 880 cm^{-1} peak is also found in SiO_x microtrees,[75] produced by the excimer laser processing of Si in air, as well as in O_2 plasma-treated Si surfaces [Fig. 2(b)], and surfaces produced by the CO_2 laser-provoked optical breakdown of air;[76] they do not appear in highly porous SiO_x nanoparticulate thin films[77] produced by the excimer laser ablation of a Si target in He/O_2.

As seen in Fig. 2, the enhancement of P_{2-4} over P_1, with increasing porosity (greater slopes), leads to the increased width of the composite peak from 85 cm^{-1} for a sample having 10% porosity to 210 cm^{-1} for a sample having 92% porosity. As a result, the *composite* peak maximum shifts from 1040 cm^{-1} (10% porosity) to 1075 cm^{-1} (92% porosity). This change in the relative heights of the component peaks with a change of the surface: volume ratio appears to us to be the reason for the changes seen in composite peak width and maxima, with treatment, as cited by other workers.[39–42,44,45,57]

B. Surface-enhanced PA-FTIR signal

The photoacoustic signal is due to the absorption of IR energy and its conversion to heat; at the sample surface, this heat causes an increase in the pressure above the gas, which is monitored by a sensitive microphone. The enhancement of this signal in porous solids has been known for more than 100 years,[78] and several models have been developed to describe it.[68,69,79–82] It is now known to result from the increased pressure change of the gas above the sample due to the presence of increased surface area in the gas-filled pores connected to the sample surface. Thus, the PA signal has two contributions:[68,69,81,82] a thermal component I_{th} independent of the sample porosity, and a component due to the expansion of the gas in the pores. Based on prior work on powders,[68,82] McGovern *et al.*[69] proposed the following model for this signal enhancement:

$$I = A\left[I_{\text{th}} + \frac{\varepsilon}{(1-\varepsilon)\alpha_a^0}\left[1 - e^{-(1-\epsilon)\alpha_a^0 l}\right]\right], \tag{1}$$

where A is a constant which depends on several components: the static gas pressure in the cell, the light absorption coefficient of the sample, the cell temperature, the heat capacity of the solid, and the cell volume.[69] I_{th} is the contribution of the thermal portion of the PA signal, which is independent of the sample porosity, α_a^0 is the optical absorption coefficient of the sample, ϵ is the sample porosity, and l is the sample thickness. Because we use the same mass thickness (i.e., thickness at zero porosity) l_0 (200 nm) for each sample, the apparent thickness l can be expressed as

$$l = l_0 \frac{1}{1-\epsilon}. \tag{2}$$

We take the thickness of the SiO_x coating into account[72] (SiO_x/Si is assumed to be spherical) as

$$d = d_0 \varepsilon^{0.8}, \tag{3}$$

where d is the SiO_x coating thickness,[72] and the power 0.8 comes from an experimental fit of the porosity data;[72] converting the sample thickness into porosity by Eq. (2), we plot the theoretical model of Eq. (1) in Fig. 3. The resultant plot, using the signal from sample F, a 250 nm nonporous SiO_2 thin film, as the thermal contribution I_{th}, shows our experimental data to be in excellent agreement with the theoretical model.

It is important to note that our semilogarithmic experimental results, in Fig. 3, are identical to the experimental results obtained for the gas permeabilities of H_2 and air in SiO_x/Si films,[83] indicating that the pores formed in our study are open cell. It is also a further confirmation that the enhanced PA-FTIR intensity comes from gas expansion in those pores. In contradistinction, there is no significant enhancement of the PA-FTIR signal intensity in the transmission FTIR spectra of porous SiO_x thin films.[45]

While we are limited in attributing the Si–O–Si stretching peaks to specific chemical structures, there are certain aspects of their behaviors that have been revealed by our data: (1) there appear to be four peaks contributing to the composite at 1045 cm^{-1} (P_1), 1060 cm^{-1} (P_2), 1090 cm^{-1} (P_3), and 1170 cm^{-1} (P_4); (2) P_{2-4} are surface related; (3) P_1, which is also present in nonporous material, is less influenced by porosity here than the other components and may not be related to the surface area, implying that it may be volume related and undergo some minor surface enhancement; (4) the different positions of P_{2-4} may be related to different chain terminations (e.g., Si–OH and $Si-CH_3$) and/or surface structures.

Although our ability to attribute the source of the PL from our PA and previously published transmission FTIR studies is limited, we may combine our previous PL study[31] with literature PL results[18,84] to note that (a) the PL intensity increases with porosity (after correcting mass), and (b) the PL peak energy decreases from ~2.3 to 1.6 eV with increasing porosity. As we have already proposed,[77] the band near 2.3 eV appears to be associated with oxide-related defect states in the volume, the peak energy changing with x in SiO_x, while the band near 1.5 eV is associated with surface states. Therefore, both the oxide-related defect state concentration (shell thickness) and the surface area increase with

increasing porosity, which serves to increase the PL intensity. At the same time, the x value increases with increasing porosity,[72] shifting the peak energy.

V. CONCLUSIONS

We have found that the asymmetric Si–O–Si stretching peak, a composite in the range of 1000–1300 cm^{-1}, contains four clearly discernable peaks, one of which (P_1) may come from the sample volume and the others (P_{2-4}) certainly come from the sample surface. The enhanced PA signal is in good agreement with the previously proposed theoretical model of McGovern *et al.*,[69] in which signal enhancement comes from gas expansion in the sample pores. High porosity Si thin films may serve as substrates for PA-FTIR chemical sensors for trace materials.

ACKNOWLEDGMENTS

The authors thank the Natural Sciences and Engineering Research Council of Canada for funding, and Vincent Ethier for sample preparation.

[1]L. Pavesi, L. Dal Negro, C. Mazzolenl, G. Franzo, and F. Priolo, Nature (London) **408**, 440 (2000).
[2]V. S.-Y. Lin, K. Motesharei, K. P. S. Dancil, M. J. Sailor, and M. R. Ghadiri, Science **278**, 840 (1997).
[3]Y. Kanemitsu, Phys. Rep. **263**, 1 (1995).
[4]A. G. Gullis, L. T. Canham, and P. D. J. Calcott, J. Appl. Phys. **82**, 909 (1997).
[5]S. M. Prokes, Appl. Phys. Lett. **62**, 3244 (1993).
[6]K. S. Min, K. V. Shcheglov, C. M. Yang, H. A. Atwater, M. L. Brongersma, and A. Polman, Appl. Phys. Lett. **69**, 2033 (1996).
[7]M. Ehbrecht, B. Kohn, F. Huisken, M. A. Laguna, and V. Paillard, Phys. Rev. B **56**, 6958 (1997).
[8]G. Ledoux, J. Gong, and F. Huisken, Appl. Phys. Lett. **79**, 4028 (2001).
[9]I. Umezu, K.-I. Yoshida, N. Sakamoto, T. Murota, Y. Takashima, M. Inada, and A. Sugimura, J. Appl. Phys. **91**, 2009 (2002).
[10]L. T. Canham, Appl. Phys. Lett. **57**, 1046 (1990).
[11]B. Delley and E. F. Steigmeier, Phys. Rev. B **47**, 1397 (1993).
[12]M. S. Brandt, H. D. Fuchs, M. Stutzmann, J. Weber, and M. Cardona, Solid State Commun. **81**, 307 (1992).
[13]C. Tsai *et al.*, Appl. Phys. Lett. **60**, 1700 (1992).
[14]S. M. Prokes and W. E. Carlos, J. Appl. Phys. **78**, 2671 (1992); L. N. Dinh, L. L. Chase, M. Balooch, L. J. Terminello, and F. Wooten, Appl. Phys. Lett. **65**, 3111 (1994); T. Torchynska *et al.*, Physica B **308**, 1108 (2002).
[15]Y. Kanemitsu, T. Futagi, T. Matsumoto, and H. Mimura, Phys. Rev. B **49**, 14732 (1994).
[16]G. Allan, C. Delerue, and M. Lannoo, Phys. Rev. Lett. **76**, 2961 (1996).
[17]J. L. Gole, F. P. Dudel, L. Seals, M. Reiger, P. Kohl, and L. A. Bottomley, J. Electrochem. Soc. **145**, 3284 (1998).
[18]M. V. Wolkin, J. Jorne, P. M. Fauchet, G. Allan, and C. Delerue, Phys. Rev. Lett. **82**, 197 (1999).
[19]S. Hayashi, S. Tanimoto, and K. Yamamoto, J. Appl. Phys. **68**, 5300 (1990).
[20]P. Melinon *et al.*, J. Chem. Phys. **107**, 10278 (1997).
[21]K. Furnkawa, Y. C. Liu, H. Nakashima, D. W. Gao, K. Uchino, K. Muraoka, and H. Tuzuki, Appl. Phys. Lett. **72**, 725 (1998).
[22]T. Makino, Y. Yamada, N. Suzuki, T. Yoshida, and S. Onari, J. Appl. Phys. **90**, 5075 (2001).
[23]S.-T. Li, S. J. Silvers, and M. S. El-Shal, J. Phys. Chem. B **101**, 1794 (1997).
[24]A. Brun-Bruneau, D. Souche, S. Fisson, V. N. Van, G. Vuye, F. Abeles, and J. Rivory, J. Vac. Sci. Technol. A **16**, 2281 (1998).
[25]S. Charvet, R. Madelon, R. Rizk, B. Garrido, O. Gonzalez-Varona, M. Lopez, A. Perez-Rodriguez, and J. R. Morante, J. Lumin. **80**, 241 (1999).
[26]E. Werwa, A. A. Seraphin, L. A. Chiu, C. Zhou, and K. D. Kolenbrander, Appl. Phys. Lett. **64**, 1821 (1994).
[27]I. A. Movtchan, R. W. Dreyfus, W. Marine, M. Sentis, M. Autric, G. Le Lay, and N. Merk, Thin Solid Films **255**, 286 (1995).
[28]Y. Yamada, T. Orii, I. Umezu, S. Takeyama, and T. Yoshida, Jpn. J. Appl. Phys., Part 1 **35**, 1361 (1996).
[29]T. Makimura, Y. Kunii, and K. Murakami, Jpn. J. Appl. Phys., Part 1 **35**, 4780 (1996).
[30]L. Patrone, D. Nelson, V. I. Safarov, M. Sentis, W. Marine, and S. Giorgio, J. Appl. Phys. **87**, 3829 (2000).
[31]A. V. Kabashin, J.-P. Sylvestre, S. Patskovsky, and M. Meunier, J. Appl. Phys. **91**, 3248 (2002).
[32]A. V. Kabashin, M. Meunier, and R. Leonelli, J. Vac. Sci. Technol. B **19**, 2217 (2001).
[33]G. Ledoux, O. Guillois, D. Porterat, C. Reynaud, F. Huisken, B. Kohn, and V. Paillard, Phys. Rev. B **62**, 15942 (2000).
[34]T. Yoshida, S. Takeyama, Y. Yamada, and K. Mutoh, Appl. Phys. Lett. **68**, 1772 (1996).
[35]L. Patrone, D. Nelson, V. I. Safarov, M. Sentis, W. Marine, and S. Giorgio, J. Appl. Phys. **87**, 3829 (2000).
[36]I. Umezu, K. Shibata, S. Yamaguchi, A. Sugimura, Y. Yamada, and T. Yoshida, J. Appl. Phys. **84**, 6448 (1998).
[37]See, e.g., L. J. Bellamy, *The Infra-Red Spectra of Complex Molecules* (Wiley, New York, 1959), Chap. 20.3 and references therein.
[38]H. Wagner and W. Beyer, Solid State Commun. **48**, 585 (1983).
[39]P. G. Pai, S. S. Chao, and Y. Takagi, J. Vac. Sci. Technol. A **4**, 689 (1986).
[40]I. W. Boyd, Appl. Phys. Lett. **51**, 418 (1987).
[41]I. W. Boyd, J. Appl. Phys. **62**, 3195 (1987).
[42]R. M. Almeida and C. G. Pantano, J. Appl. Phys. **68**, 4225 (1990).
[43]H. D. Fuchs, M. Stutzmann, M. S. Brandt, M. Rosenbauer, J. Weber, A. Breitschwerdt, P. Deàk, and M. Cardonna, Phys. Rev. B **48**, 8172 (1993).
[44]I. Montero, L. Galán, O. Najmi, and J. M. Albella, Phys. Rev. B **50**, 4881 (1994).
[45]J.-S. Chou and S.-C. Lee, J. Appl. Phys. **77**, 1805 (1995).
[46]J. M. Rehm, G. L. McLendon, L. Tsybeskov, and P. M. Fauchet, Appl. Phys. Lett. **66**, 3669 (1995).
[47]E. I. Kamitsos, Phys. Rev. B **53**, 14659 (1996).
[48]R. M. Almeida, Phys. Rev. B **53**, 14656 (1996).
[49]S. E. Babayan and J. Y. Jeong, Plasma Sources Sci. Technol. **7**, 286 (1998).
[50]J. Eng, Jr., *et al.*, J. Chem. Phys. **108**, 8680 (1998).
[51]M. J. Loboda, C. M. Grove, and R. F. Schneider, J. Electrochem. Soc. **145**, 2861 (1998).
[52]R. R. Lowe-Webb, H. Lee, J. B. Ewing, S. R. Collins, W. Yang, and P. C. Sercel, J. Appl. Phys. **83**, 2815 (1998).
[53]J. J. Senkevich and S. B. Desu, Thin Solid Films **322**, 148 (1998).
[54]J. Wang, B. Zou, and M. A. El-Sayed, J. Mol. Struct. **508**, 87 (1999).
[55]W.-C. Chen, S.-C. Lin, B.-T. Dai, and M.-S. Tsai, J. Electrochem. Soc. **146**, 3004 (1999).
[56]N. E. Korunskaya, T. V. Torchinskaya, L. Yu. Khomenkova, B. R. Dzhumaev, and S. M. Prokes, Microelectron. Eng. **51–52**, 485 (2000).
[57]K. T. Queeney, M. K. Weldon, J. P. Chang, Y. J. Chabal, A. B. Gurevich, J. Sapjeta, and R. L. Opila, J. Appl. Phys. **87**, 1322 (2000).
[58]M. K. Gunde, Physica B **292**, 286 (2000).
[59]C. Y. Wang, Z. X. Shen, and J. Z. Zheng, Appl. Spectrosc. **54**, 209 (2000).
[60]K. Ragavachari and J. Eng, Jr., Phys. Rev. Lett. **84**, 935 (2000).
[61]S. E. Babayan, J. Y. Jeong, A. Schütze, V. J. Tu, M. Moravej, G. S. Selwyn, and R. F. Hicks, Plasma Sources Sci. Technol. **10**, 573 (2001).
[62]G. Pérez and J. M. Sanz, Thin Solid Films **416**, 24 (2002).
[63]P. Innocenzi, J. Non-Cryst. Solids **316**, 309 (2003).
[64]T. Minami, T. Utsubo, T. Yamatani, T. Miyata, and Y. Ohbayashi, Thin Solid Films **426**, 47 (2003).
[65]V. E. Vamvakas and D. Davazoglu, J. Electrochem. Soc. **151**, F93 (2004).
[66]S. Yu, K. S. Wong, X. Hu, K. Pita, and V. Ligatchev, J. Electrochem. Soc. **151**, F123 (2004).
[67]D. D. Burkey and K. K. Gleason, J. Vac. Sci. Technol. A **22**, 61 (2004).
[68]J. P. Monchalin, L. Bertrand, G. Rousset, and S. Lepoutre, J. Appl. Phys. **56**, 190 (1984).
[69]S. J. McGovern, B. S. H. Royce, and J. B. Benziger, J. Appl. Phys. **57**, 1710 (1985).
[70]U. Bernini, P. Maddalena, E. Massera, and A. Ramaglia, J. Opt. A, Pure Appl. Opt. **1**, 210 (1999).
[71]D.-Q. Yang, J.-N. Gillet, M. Meunier, and E. Sacher, J. Appl. Phys. **97**, 024303 (2005).
[72]D.-Q. Yang, M. Meunier, and E. Sacher, J. Appl. Phys. (submitted).

[73]M. Zacharias, D. Dimova-Malinovska, and M. Stutzmann, Philos. Mag. B **73**, 799 (1996); B. Gelloz and N. Koshida, J. Appl. Phys. **88**, 4319 (2000); L. X. Yi, J. Heitman, R. Scholz, and M. Zacharias, Appl. Phys. Lett. **81**, 4248 (2002).
[74]D.-Q. Yang, E. Sacher, and M. Meunier, J. Appl. Phys. **95**, 5023 (2004); D.-Q. Yang, E. Sacher, and M. Meunier, Appl. Phys. A: Mater. Sci. Process. **80**, 575 (2005).
[75]D.-Q. Yang, E. Sacher, and M. Meunier, Proc. SPIE **5578**, 652 (2004).
[76]D.-Q. Yang, A. V. Kabashin, V.-G. Pilon-Marien, E. Sacher, and M. Meunier, J. Appl. Phys. **95**, 5722 (2004).
[77]D.-Q. Yang, V. Ethier, E. Sacher, and M. Meunier, J. Appl. Phys. **98**, 024310 (2005).
[78]A. G. Bell, Philos. Mag. **11**, 510 (1881).
[79]A. Rosencwaig and A. Gersho, J. Appl. Phys. **47**, 64 (1976).
[80]J. Pelzl, K. Klein, and O. Hordhaus, Appl. Opt. **21**, 94 (1982).
[81]F. A. McDonald and J. C. Wetsel, Jr., J. Appl. Phys. **49**, 2313 (1978).
[82]Z. A. Yasa, W. A. Jackson, and N. M. Amer, Appl. Opt. **21**, 21 (1982).
[83]A. Koponen, M. Kataja, and J. Timonen, Phys. Rev. E **56**, 3319 (1997); V. Lysenko, J. Vitiello, B. Remaki, and D. Barbier, *ibid.* **70**, 017301 (2004).
[84]P. M. Fauchet and J. Von Behren, Phys. Status Solidi B **204**, R7 (1997).